Supplementary Material: Nuclear Quantum Effects in Gas-Phase Ethylene Glycol

Mrinal Arandhara and Sai G. Ramesh*

Department of Inorganic and Physical Chemistry, Indian Institute of Science, Bangalore 560012

TABLE S-1. Ab initio energies at the local minima and TS geometries of EG at various levels of theory.

	tG^+g^-	$g^+G^+g^-$	$g^-G^+g^-$	tTt	g^+Tg^-	tTg^+	g^+Tg^+	tG^+t	tG^+g^+	cCt
MP2/aVDZ	0.0	149.8	357.4	900.8	984.4	972.4	1045.4	1091.9	1240.7	2427.1
CCSD(T)/aVDZ//MP2/aVDZ	0.0	111.6	304.5	877.3	907.0	918.8	966.7	1094.6	1210.9	2323.7
MP2/aVTZ	0.0	148.9	330.2	912.1	979.0	971.0	1045.9	1084.2	1248.6	2298.3
CCSD/aVDZ	0.0	142.9	322.2	819.0	904.3	888.8	970.2	1065.8	1200.9	2352.3
CCSD(T)/aVDZ//CCSD/aVDZ	0.0	112.8	304.8	876.1	907.9	918.5	967.6	1092.9	1209.9	2323.7

TABLE S-2. Energies and geometries of stationary points of EG at the MP2/aVTZ level of theory. See also Table 1 in the main manuscript. All bond lengths are in Å while all angles and dihedrals are in degrees. Equivalent structures that have the same energy are obtained by the transformations $(\phi_1, \phi_2, \phi_3) \rightarrow (-\phi_1, -\phi_2, -\phi_3)$ and $(\phi_1, \phi_2, \phi_3) \rightarrow (\phi_1, \phi_3, \phi_2)$ with attendant changes in internals, some of which remain the same and others are exchanged.

		tG^+g^-	$g^+G^+g^-$	$g^-G^+g^-$	tTt	g^+Tg^-	tTg^+	g^+Tg^+	tG^+t	tG^+g^+	cCt
ϕ_1	$\phi(O_3C_1C_2O_4)$	62.15	57.68	60.53	180.0	180.0	179.65	176.66	73.93	65.30	0.0
ϕ_2	$\phi(H_9O_3C_1C_2)$	−168.65	73.91	−80.11	180.0	70.63	−175.90	67.26	−168.17	-178.37	0.0
ϕ_3	$\phi(H_{10}O_4C_2C_1)$	−51.97	−44.88	−80.11	180.0	−70.63	71.91	67.26	−168.17	59.51	180.0
E		0.00	148.9	330.2	912.1	979.0	971.0	1045.9	1084.2	1248.6	2298.3
R_1	$r(C_2C_1)$	1.5087	1.5125	1.5128	1.5102	1.5195	1.5151	1.5192	1.5052	1.5104	1.5488
R_2	$r(O_3C_1)$	1.4303	1.4305	1.4260	1.4249	1.4235	1.4243	1.4226	1.4235	1.4206	1.4163
R_3	$r(O_4C_2)$	1.4187	1.4175	1.4260	1.4249	1.4235	1.4233	1.4226	1.4235	1.4197	1.4287
R_4	$r(H_5C_2)$	1.0942	1.0970	1.0923	1.0923	1.0924	1.0877	1.0877	1.0927	1.0885	1.0907
R_5	$r(H_6C_2)$	1.0888	1.0898	1.0899	1.0923	1.0901	1.0923	1.0956	1.0943	1.0950	1.0907
R_6	$r(H_7C_1)$	1.0935	1.0930	1.0899	1.0923	1.0924	1.0953	1.0956	1.0943	1.0953	1.0908
R_7	$r(H_8C_1)$	1.0922	1.0882	1.0923	1.0923	1.0901	1.0922	1.0877	1.0927	1.0964	1.0908
R_8	$r(H_9O_3)$	0.9616	0.9633	0.9623	0.9615	0.9625	0.9617	0.9627	0.9614	0.9619	0.9663
R_9	$r(H_{10}O_4)$	0.9651	0.9659	0.9623	0.9615	0.9625	0.9623	0.9627	0.9614	0.9627	0.9613
R_{10}	$\theta(O_3C_1C_2)$	106.0	110.5	111.3	106.5	111.6	106.7	111.7	108.3	108.6	113.2
R_{11}	$\theta(O_4C_2C_1)$	111.3	111.1	111.3	106.5	111.6	111.3	111.7	108.3	113.7	107.9
R_{12}	$\theta(H_5C_2C_1)$	109.1	109.6	109.7	109.3	109.6	109.5	109.5	108.6	109.1	110.2
R_{13}	$\theta(H_6C_2C_1)$	109.9	110.2	109.8	109.3	109.9	109.6	110.0	108.9	108.6	110.2
R_{14}	$\theta(H_7C_1C_2)$	110.1	110.7	109.8	109.3	109.6	109.6	110.0	108.9	108.4	109.3
R_{15}	$\theta(H_8C_1C_2)$	109.6	109.8	109.7	109.3	109.9	109.3	109.5	108.6	109.5	109.3
R_{16}	$\theta(H_9O_3C_1)$	108.8	108.0	107.2	108.3	108.1	108.5	108.2	108.5	108.4	106.6
R_{17}	$\phi(H_{10}O_4C_2)$	105.9	105.9	107.2	108.3	108.1	108.1	108.2	108.5	108.1	108.7
R_{18}	$\phi(H_5C_2C_1O_4)$	−122.7	−122.6	−122.9	−120.6	−124.5	−117.4	−117.6	−121.1	−117.7	−120.1
R_{19}	$\phi(H_6C_2C_1O_4)$	118.3	118.6	117.9	120.6	117.1	124.2	124.1	120.5	124.4	120.1
R_{20}	$\phi(H_7C_1C_2O_3)$	120.1	123.8	117.9	120.6	124.5	120.4	124.1	120.5	120.9	121.1
R_{21}	$\phi(H_8C_1C_2O_3)$	−119.5	−115.9	−122.9	−120.6	−117.1	−121.1	−117.6	−121.0	−121.4	−121.1
Equiv. struct.		tG^-g^+ g^+G^-t g^-G^+t	$g^-G^-g^+$ $g^+G^-g^-$ $g^-G^+g^+$	$g^+G^-g^+$		g^-Tg^+	tTg^- g^-Tt g^+Tt	g^-Tg^-	tG^-t	tG^-g^- g^-G^-t g^+G^+t	tCc

* Corresponding author. Emails: (MA) mrinala@iisc.ac.in; (SGR) sairamesh@iisc.ac.in

TABLE S-3. Normal mode frequencies of EG, computed at the minima with the MP2/aug-cc-pVTZ level of theory.

NM	tG^+g^-	$g^+G^+g^-$	$g^-G^+g^-$	tTt	g^+Tg^-	tTg^+	g^+Tg^+	tG^+t	tG^+g^+	cCt
ϕ_1	62.15	57.68	60.53	180.0	180.0	179.65	176.66	73.93	65.30	0.0
ϕ_2	−168.65	73.91	−80.11	180.0	70.63	−175.90	67.26	−168.17	−178.37	0.0
ϕ_3	−51.97	−44.88	−80.11	180.0	−70.63	71.91	67.26	−168.17	59.51	180.0
ω_1	168.4	167.8	99.8	115.9	141.0	129.4	145.0	152.1	132.8	i238.6
ω_2	247.2	292.1	158.9	216.5	250.1	227.9	250.0	185.5	227.2	i27.1
ω_3	328.6	326.8	320.9	230.0	268.1	262.3	264.2	192.6	238.0	323.9
ω_4	419.5	452.0	428.1	291.0	295.9	293.3	304.9	337.5	331.8	345.7
ω_5	523.2	535.5	527.5	481.4	475.2	478.8	475.6	495.4	509.8	612.7
ω_6	886.9	877.8	880.7	838.9	802.5	820.4	804.4	900.7	886.2	871.9
ω_7	903.8	897.4	885.4	1008.9	1026.5	1022.1	1042.8	915.9	900.2	899.0
ω_8	1065.9	1059.4	1051.2	1076.3	1073.8	1079.8	1048.5	1058.8	1058.3	1087.2
ω_9	1099.6	1073.4	1063.3	1094.0	1090.4	1082.4	1091.2	1100.9	1097.1	1106.9
ω_{10}	1129.5	1122.0	1126.1	1167.0	1109.2	1104.4	1109.2	1127.0	1131.3	1159.9
ω_{11}	1178.4	1203.7	1197.7	1190.0	1140.4	1213.1	1158.3	1215.8	1195.9	1213.0
ω_{12}	1268.8	1245.8	1257.4	1235.1	1319.7	1240.3	1303.9	1257.0	1253.4	1280.6
ω_{13}	1296.3	1373.8	1383.0	1288.0	1339.2	1321.4	1347.5	1298.0	1322.1	1301.3
ω_{14}	1384.4	1377.3	1388.5	1319.2	1370.1	1367.9	1385.7	1329.6	1381.5	1331.1
ω_{15}	1419.9	1405.6	1404.0	1409.3	1404.2	1393.1	1387.7	1429.2	1419.1	1442.3
ω_{16}	1454.8	1435.4	1421.7	1486.5	1432.8	1462.3	1432.8	1482.8	1461.7	1465.3
ω_{17}	1515.5	1511.5	1508.2	1541.0	1521.2	1529.3	1521.2	1519.3	1509.7	1542.9
ω_{18}	1523.5	1520.9	1512.1	1550.7	1534.9	1543.3	1534.7	1520.0	1523.4	1563.8
ω_{19}	3053.1	3026.2	3070.6	3056.8	3067.1	3037.6	3040.8	3040.6	3021.7	3064.8
ω_{20}	3058.1	3069.9	3073.5	3063.6	3075.7	3076.5	3042.5	3050.3	3049.9	3076.4
ω_{21}	3114.1	3133.7	3139.9	3101.9	3124.2	3102.2	3149.7	3098.2	3073.9	3101.8
ω_{22}	3149.4	3158.8	3147.8	3127.3	3149.6	3163.5	3166.0	3110.0	3152.0	3131.2
ω_{23}	3808.1	3793.7	3845.0	3857.2	3840.3	3843.8	3837.9	3855.4	3836.4	3771.3
ω_{24}	3855.6	3830.5	3846.4	3858.0	3841.7	3854.5	3839.0	3855.4	3850.1	3863.6

Symmetry-adapted Fourier expansions in ϕ_1, ϕ_2, ϕ_3 space:

$$
\begin{aligned}
Y^{(es)}(\phi_1,\phi_2,\phi_3) = \quad & \sum_{m\geq 0}^{M}\sum_{n\geq 0}^{N} A_{mn}^{(es,1)} \cos(m\phi_1)\cos(n\phi_2)\cos(n\phi_3) \\
& + \sum_{m\geq 0}^{M}\sum_{n\geq 0}^{N}\sum_{l\geq 0}^{n-1} A_{mnl}^{(es,2)} \cos(m\phi_1)\left[\cos(n\phi_2)\cos(l\phi_3)+\cos(l\phi_2)\cos(n\phi_3)\right] \\
& + \sum_{m\geq 0}^{M}\sum_{n> 0}^{N} A_{mn}^{(es,3)} \cos(m\phi_1)\sin(n\phi_2)\sin(n\phi_3) \\
& + \sum_{m\geq 0}^{M}\sum_{n> 0}^{N}\sum_{l> 0}^{n-1} A_{mnl}^{(es,4)} \cos(m\phi_1)\left[\sin(n\phi_2)\sin(l\phi_3)+\sin(l\phi_2)\sin(n\phi_3)\right] \\
& + \sum_{m> 0}^{M}\sum_{n\geq 0}^{N}\sum_{l> 0}^{N} A_{mnl}^{(es,5)} \sin(m\phi_1)\left[\cos(n\phi_2)\sin(l\phi_3)+\sin(l\phi_2)\cos(n\phi_3)\right],
\end{aligned}
\tag{S1a}
$$

$$
\begin{aligned}
Y^{(ea)}(\phi_1,\phi_2,\phi_3) = \quad & \sum_{m\geq 0}^{M}\sum_{n> 0}^{N}\sum_{l\geq 0}^{n-1} A_{mnl}^{(ea,1)} \cos(m\phi_1)\left[\cos(n\phi_2)\cos(l\phi_3)-\cos(l\phi_2)\cos(n\phi_3)\right] \\
& + \sum_{m\geq 0}^{M}\sum_{n> 1}^{N}\sum_{l> 0}^{n-1} A_{mnl}^{(ea,2)} \cos(m\phi_1)\left[\sin(n\phi_2)\sin(l\phi_3)-\sin(l\phi_2)\sin(n\phi_3)\right] \\
& + \sum_{m> 0}^{M}\sum_{n\geq 0}^{N}\sum_{l> 0}^{N} A_{mnl}^{(ea,3)} \sin(m\phi_1)\left[\cos(n\phi_2)\sin(l\phi_3)-\sin(l\phi_2)\cos(n\phi_3)\right],
\end{aligned}
\tag{S1b}
$$

$$
\begin{aligned}
Y^{(os)}(\phi_1,\phi_2,\phi_3) = \quad & \sum_{m> 0}^{M}\sum_{n\geq 0}^{N} f_{mnl}^{(os,1)} \sin(m\phi_1)\cos(n\phi_2)\cos(n\phi_3) \\
& + \sum_{m> 0}^{M}\sum_{n\geq 0}^{N}\sum_{l\geq 0}^{n-1} f_{mnl}^{(os,2)} \sin(m\phi_1)\left[\cos(n\phi_2)\cos(l\phi_3)+\cos(l\phi_2)\cos(n\phi_3)\right] \\
& + \sum_{m> 0}^{M}\sum_{n> 0}^{N} f_{mnl}^{(os,3)} \sin(m\phi_1)\sin(n\phi_2)\sin(n\phi_3) \\
& + \sum_{m> 0}^{M}\sum_{n> 0}^{N}\sum_{l> 0}^{n-1} f_{mnl}^{(os,4)} \sin(m\phi_1)\left[\sin(n\phi_2)\sin(l\phi_3)+\sin(l\phi_2)\sin(n\phi_3)\right] \\
& + \sum_{m\geq 0}^{M}\sum_{n\geq 0}^{N}\sum_{l> 0}^{N} f_{mnl}^{(os,5)} \cos(m\phi_1)\left[\cos(n\phi_2)\sin(l\phi_3)+\sin(l\phi_2)\cos(n\phi_3)\right],
\end{aligned}
\tag{S1c}
$$

$$
\begin{aligned}
Y^{(oa)}(\phi_1,\phi_2,\phi_3) = \quad & \sum_{m> 0}^{M}\sum_{n> 0}^{N}\sum_{l\geq 0}^{n-1} f_{mnl}^{(oa,1)} \sin(m\phi_1)\left[\cos(n\phi_2)\cos(l\phi_3)-\cos(l\phi_2)\cos(n\phi_3)\right] \\
& + \sum_{m> 0}^{M}\sum_{n> 1}^{N}\sum_{l> 0}^{n-1} f_{mnl}^{(oa,2)} \sin(m\phi_1)\left[\sin(n\phi_2)\sin(l\phi_3)-\sin(l\phi_2)\sin(n\phi_3)\right] \\
& + \sum_{m\geq 0}^{M}\sum_{n\geq 0}^{N}\sum_{l> 0}^{N} f_{mnl}^{(oa,3)} \cos(m\phi_1)\left[\cos(n\phi_2)\sin(l\phi_3)-\sin(l\phi_2)\cos(n\phi_3)\right].
\end{aligned}
\tag{S1d}
$$

TABLE S-4. Definitions of the symmetrized internal coordinates of EG.

Coord.	Definition	Sym.	Coord.	Definition	Sym.
S_1	R_1	es	S_{12}	$(R_{12}+R_{13}+R_{14}+R_{15})/2$	es
S_2	$(R_2+R_3)/\sqrt{2}$	es	S_{13}	$(R_{12}-R_{13}+R_{14}-R_{15})/2$	oa
S_3	$(R_2-R_3)/\sqrt{2}$	ea	S_{14}	$(R_{12}-R_{13}-R_{14}+R_{15})/2$	os
S_4	$(R_4+R_5+R_6+R_7)/2$	es	S_{15}	$(R_{12}+R_{13}-R_{14}-R_{15})/2$	ea
S_5	$(R_4-R_5+R_6-R_7)/2$	oa	S_{16}	$(R_{16}+R_{17})/\sqrt{2}$	es
S_6	$(R_4-R_5-R_6+R_7)/2$	os	S_{17}	$(R_{16}-R_{17})/\sqrt{2}$	ea
S_7	$(R_4+R_5-R_6-R_7)/2$	ea	S_{18}	$(R_{18}+R_{19}+R_{20}+R_{21})/2$	os
S_8	$(R_8+R_9)/\sqrt{2}$	es	S_{19}	$(R_{18}-R_{19}+R_{20}-R_{21})/2$	ea
S_9	$(R_8-R_9)/\sqrt{2}$	ea	S_{20}	$(R_{18}-R_{19}-R_{20}+R_{21})/2$	es
S_{10}	$(R_{10}+R_{11})/\sqrt{2}$	es	S_{21}	$(R_{18}+R_{19}-R_{20}-R_{21})/2$	oa
S_{11}	$(R_{10}-R_{11})/\sqrt{2}$	ea			

TABLE S-5. Ranges of one-dimensional displacements along bonds (R_1-R_9, in Å) and angles (R_{10}-R_{17}, in degrees) from the reaction surface towards the calculation of quintic up to octic force constants.

Bonds	R_{min}	R_{max}	δR	Angles[a,b]	R_{min}	R_{max}	δR
R_1	−0.225	0.300	0.025	R_{10}	−17.5	30.0	2.5
R_2	−0.225	0.250	0.025	R_{11}	−25.0	22.5	2.5
R_3	−0.225	0.275	0.025	R_{12}	−32.0	40.0	4.0
R_4	−0.320	0.400	0.040	R_{13}	−32.0	40.0	4.0
R_5	−0.320	0.400	0.040	R_{14}	−36.0	36.0	4.0
R_6	−0.320	0.400	0.040	R_{15}	−36.0	36.0	4.0
R_7	−0.320	0.400	0.040	R_{16}	−40.0	40.0	4.0
R_8	−0.280	0.400	0.040	R_{17}	−36.0	40.0	4.0
R_9	−0.280	0.400	0.040				

[a] For R_{10} and R_{10}, at some points in (ϕ_1, ϕ_2, ϕ_3) space, the above ranges gave poorer fits. Hence the ranges were slighly reduced from both ends by the removal of 3 points in total.

[b] For R_{12}-R_{15}, selected dihedral points were excluded due to high energies resulting from the displacement.

TABLE S-6. Root mean square errors for fits of optimal values of symmetrized internals S_j° on the reaction surface. Based on the mode symmetries (Table S-4), the appropriate symmetry-adapted expressions from Eqs. (S1a)-(S1d) were used. In all cases, $(M, N) = (9, 7)$ was used.

Bonds	RMSE (Å, $\times 10^{-5}$)	Angles	RMSE (°, $\times 10^{-3}$)	Dihedrals	RMSE (°, $\times 10^{-3}$)
S_1°	0.71	S_{10}°	4.86	S_{18}°	1.59
S_2°	0.77	S_{11}°	0.70	S_{19}°	0.95
S_3°	1.00	S_{12}°	1.99	S_{20}°	2.24
S_4°	0.16	S_{13}°	0.70	S_{21}°	0.86
S_5°	0.10	S_{14}°	1.69		
S_6°	0.14	S_{15}°	0.82		
S_7°	0.19	S_{16}°	4.18		
S_8°	1.67	S_{17}°	2.75		
S_9°	1.43				

S1. GENERATION OF THE SET OF TEST DATA POINTS FOR ETHYLENE GLYCOL

As a test of the quality of the potential surface, we have compared the energies and forces obtained from our PES with ab initio values at the MP2/aVTZ level of theory at 15150 geometries. These were sampled from a combination of methods as follows.

1. Sampling from the quantum harmonic distribution, as discussed by Brown.[1] This is used at each of the 9 minima as well as the cCt and cCc geometries. For the last two, the magnitudes of the imaginary frequencies were considered for sampling purposes. Using control parameters A with values of 0.5, 1, and 2, we have obtained 1000 points per region, i.e. a total of 11000 points. Care was taken that internal variables are sampled sufficiently widely but not over-extended and also that no two geometries are too close to each other, as measured by the 'distance' in bond-angle-dihedral space. As also used in our recent study on 2-fluoroethanol,[2] vectors are composed of bond distances, angles and dihedrals for each geometry. Magnitudes of difference vectors between each pair of points are calculated. Denoting these as l_b, l_a and l_d for a pair of geometries, it was ensured for the 11000 points selected that at least two of the following criteria were satisfied: $l_b > 0.2$ Å, $l_b > 5°$ and $l_d > 15°$. As this approach yields points near the stationary points, subsequent sampling was focused on regions away from such points.

2. PIMD trajectories at 300 K with the auxilliary MP2/aVDZ PES including up to octic order terms. Data are sampled from selected beads along a 2 ns trajectory every 50 fs. The collected geometries are filtered based on the bond-angle-dihedral proximity criteria. From the geometries that remained, points were sampled based on values in ϕ_1 and ϕ_2 (note that ϕ_3 was not specially considered owing to its formal equivalence to ϕ_2). (a) 500 points were sampled for ϕ_1 in the range [0°, 40°] and [80°, 100°] and without restriction on ϕ_2. (b) For ϕ_1 outside this range, 500 points were sampled for ϕ_2 in the ranges [−130°, −95°] and [−15°, 30°]. (c) 1000 points in the rest of the ϕ_2 space with ϕ_1 again outside the ranges given in (a). The sample sizes in these regions reflect the density of filtered points. A total of 2000 points were obtained from this approach.

3. Geometries from path integral umbrella sampling simulations along ϕ_1 using 16 beads at 300 K. Windows of 10° width, except in the ranges 40°-90° and 160°-180° were considered. From most windows and after due proximity filtering, 200 points were taken, except fewer ones from bins closest to the excluded areas. A total of 1850 points were sampled in this manner. In addition, points for $\phi_1 \in$ [145°, 180°] and $\phi_2 \in$ [−135°, 25°] (200 points) and $\in$ [105°, 140°] (100 points) were added to cover regions missed by the above sampling. In this manner, a total of 2150 test points were obtained from PI-US simulations.

The distribution of these points projected onto (ϕ_1, ϕ_2) space is shown in Fig. 3 of the main manuscript.

S2. CONVERGENCE OF PATH INTEGRAL SIMULATIONS WITH RESPECT TO NUMBER OF BEADS P

Presented in Tables S-7 and S-8 are the checks for convergence with respect to P of the simulations at 300 K and 50 K, respectively. The quantities used for the check are the estimators for the virial kinetic and potential energies as well as selected bond lengths and angles. The average virial KE and PE estimators are defined as[3,4]

$$\langle KE_{\rm vir}\rangle = \frac{3Nk_BT}{2} + \left\langle \frac{1}{2P}\sum_{k=1}^{P}\sum_{i=1}^{N}\left(\boldsymbol{r}_i^{(k)} - \boldsymbol{r}_i^{(c)}\right)\cdot\frac{\partial V}{\partial \boldsymbol{r}_i^{(k)}}\right\rangle, \qquad \text{and} \qquad \langle V_{\rm vir}\rangle = \left\langle \frac{1}{P}\sum_{k=1}^{P} V(\boldsymbol{r}_1^{(k)},\cdots,\boldsymbol{r}_N^{(k)})\right\rangle,$$

where N and P are the total number of atoms and beads/replicas, respectively, while k_B is the Boltzmann constant and T is the temperature. The Cartesian coordinate of the $k^{\rm th}$ bead/replica of the $i^{\rm th}$ atom is denoted $\boldsymbol{r}_i^{(k)}$, and $\boldsymbol{r}_i^c$ is the centroid Cartesian coordinate of the i^{th} atom. $V(\boldsymbol{r}_1^{(k)},\cdots,\boldsymbol{r}_N^{(k)})$ is the potential energy of the k^{th} replica.

From the 300 K convergence checks in Table S-7, we see that $P = 32$ is already sufficient to converge the internals while the virial estimators are also very nearly converged. The ($P = 64, \Delta t = 0.25$ fs) results compare well both ($P = 64, \Delta t = 0.1$ fs) and ($P = 128, \Delta t = 0.1$ fs). This suggest that $P = 64$ is sufficient for the path integral

TABLE S-7. Convergence tests with respect to the number of beads P and time step in PIMD simulations at 300 K. $\langle KE_{vir}\rangle$ and $\langle V_{vir}\rangle$ are the average virial kinetic potential energy estimators. Selected internals are also listed. Simulations for these convergence tests are all 1 ns long.

P		16	32	64		128
Δt	fs	0.25	0.25	0.1	0.25	0.1
$\langle KE_{vir}\rangle$	kcal mol^{-1}	18.189	19.434	19.869	19.735	19.816
$\langle V_{vir}\rangle$	kcal mol^{-1}	26.362	27.647	28.078	27.967	27.977
$r(C_2\text{-}C_1)$	Å	1.5219	1.5225	1.5231	1.5225	1.5234
$r(O_3\text{-}C_1)$	Å	1.4353	1.4345	1.4340	1.4363	1.4349
$r(H_9\text{-}O_3)$	Å	0.9798	0.9816	0.9822	0.9811	0.9823
$r(H_{10}\text{-}O_4)$	Å	0.9796	0.9807	0.9833	0.9821	0.9814
$\theta(O_3\text{-}C_1\text{-}C_2)$	deg	109.87	110.15	110.22	109.84	110.16
$\theta(H_9\text{-}O_3\text{-}C_1)$	deg	107.58	107.41	107.47	107.61	107.23
$\theta(H_{10}\text{-}O_4\text{-}C_1)$	deg	107.40	107.54	107.61	107.27	107.58

TABLE S-8. Convergence tests with respect to the number of beads P and time step in PIMD simulations at 50 K. $\langle KE_{vir}\rangle$ and $\langle V_{vir}\rangle$ are average virial kinetic and potential energy estimators. Selected internals are also listed. Simulations for these convergence tests are all 1 ns long.

P		16	32	64		128		256	
Δt	fs	0.25	0.25	0.1	0.25	0.1	0.25	0.1	0.25
$\langle KE_{vir}\rangle$	kcal mol^{-1}	11.942	17.580	21.961	21.908	24.059	24.040	24.894	24.783
$\langle V_{vir}\rangle$	kcal mol^{-1}	13.406	19.278	23.805	23.810	26.031	26.011	26.837	26.783
$r(C_2\text{-}C_1)$	Å	1.5169	1.5186	1.5192	1.5192	1.5194	1.5192	1.5193	1.5203
$r(O_3\text{-}C_1)$	Å	1.4378	1.4396	1.4393	1.4307	1.4407	1.4383	1.4407	1.4395
$r(H_9\text{-}O_3)$	Å	0.9673	0.9715	0.9764	0.9766	0.9782	0.9791	0.9797	0.9794
$r(H_{10}\text{-}O_4)$	Å	0.9710	0.9751	0.9800	0.9787	0.9822	0.9818	0.9834	0.9836
$\theta(O_3\text{-}C_1\text{-}C_2)$	deg	106.52	106.44	106.46	107.36	106.42	107.15	106.39	106.38
$\theta(H_9\text{-}O_3\text{-}C_1)$	deg	108.81	108.78	108.82	108.33	108.74	108.39	108.72	108.83
$\theta(H_{10}\text{-}O_4\text{-}C_1)$	deg	106.17	106.23	106.28	106.63	106.03	106.52	106.15	106.14

simulations at 300 K. Also, the convergence with respect to Δt indicates indirectly that the 5 times lower time step from additional Trotter factorization for the non-centroid modes (see Sec. 2.3) is adequate. Table S-8 shows that at least $P = 128$ is required for converged results at 50 K. Once again, the similarily of the results with two time steps at both $P = 128$ and $P = 256$ again suggests the adequacy of the lower time step from the additional Trotter factorization for the non-centroid modes.

For the main results of the work, we have used $P = 64$ at 300 K and $P = 128$ at 200 K, 100 K and 50 K in the path integral simulations. The above tables suggest that these choices would yield converged results.

[1] S. E. Brown, *J. Chem. Phys.*, 2019, **151**, 194111.
[2] M. Arandhara and S. G. Ramesh, *Phys. Chem. Chem. Phys.*, 2024, **26**, 6885.
[3] M. E. Tuckerman, *Statistical Mechanics: Theory and Molecular Simulation (Oxford Graduate Texts)*, Oxford University Press, 2010.
[4] M. Shiga, *Reference Module in Chemistry, Molecular Sciences and Chemical Engineering*, Elsevier, 2018.

TABLE S-9. **Umbrella sampling parameters for PIMD and classical simulations for EG.** In all cases, the umbrella windows along ϕ_{1c} were spaced at 5° intervals between 0° and 180°. Biases of the form $V_{umb} = \frac{1}{2}K_{umb}(\phi_{1c} - \phi^{\circ}_{1c})^2$ were applied.

(1) At 300, for both PIMD and classical simulations, K_{umb} = 500 kJ mol$^{-1}rad^{-2}$ and the total simulation time T_{sim} = 200 ps. The first 10 ps were discarded.

(2) At 50 K, for undeuterated simulations, we use K =200 kJ mol^{-1}rad^{-2} and T_{sim} = 400 ps. The first 50 ps were discarded.

(3) At 50 K, for simulations with monodeuteration ($CHOD_9$ or $CHOD_{10}$, indicating that only one of the two OH hydrogen is deuterated, while CH hydrogens are not deuterated) or fully deuteration (CDOD, where all 6 H atoms of EG are deuterated), the table below provides the parameters.

The force constant and simulation length in each window were adjusted by trial-and-error to ensure that the distributions of ϕ_1 have sufficient overlap between successive windows.

ϕ°_{1c}	$CHOD_9$		$CHOD_{10}$		CDOD	
	T_{sim}	K_{umb}	T_{sim}	K_{umb}	t (ps)	K_{umb}
0	400	200	400	200	400	200
5	400	200	400	200	400	200
10	400	200	400	200	400	200
15	400	200	400	200	400	200
20	400	200	400	200	400	200
25	400	200	400	200	400	200
30	400	200	400	200	400	200
35	400	200	400	200	400	200
40	400	200	400	200	200	200
45	200	500	200	500	400	200
50	200	500	200	500	400	200
55	200	500	200	500	400	200
60	200	500	200	500	200	500
65	200	500	200	500	200	500
70	200	500	200	500	200	500
75	200	500	200	500	200	500
80	200	500	200	500	200	500
85	200	500	200	500	200	500
90	200	500	200	500	200	500
95	200	500	200	500	200	500
100	400	200	400	200	300	200
105	400	200	400	200	300	200
110	400	200	400	200	300	200
115	400	200	400	200	300	200
120	400	200	400	200	300	200
125	400	200	400	200	300	200
130	400	200	400	200	300	200
135	400	200	400	200	300	200
140	400	200	400	200	300	200
145	400	200	400	200	300	200
150	400	200	400	200	300	200
155	400	200	400	200	300	200
160	400	200	400	200	300	200
165	400	200	400	200	300	200
170	400	200	400	200	300	200
175	400	200	400	200	300	200
180	400	200	400	200	300	200

Units: T_{sim} (ps) and K_{umb} (kJ mol^{-1} rad^{-2})

TABLE S-10. Cartesian coordinates in Å of the key stationary points of EG. See also Fig 2, Table 1 and S-2.

tG$^+$g$^-$

C1	−0.67908078	0.60205726	−0.27362755
C2	0.72469313	0.56830366	0.27769448
O3	−1.32495008	−0.57555101	0.21781569
O4	1.43655931	−0.56564035	−0.19195041
H5	0.68052290	0.57711823	1.37094013
H6	1.27495187	1.44691413	−0.05495101
H7	−1.19497887	1.50332989	0.06897088
H8	−0.64376873	0.59645889	−1.36524176
H9	−2.15854557	−0.68886187	−0.24811844
H10	0.87527051	−1.32759391	−0.00292353

g$^+$G$^+$g$^-$

C1	−0.67611587	0.59765477	−0.29206028
C2	0.72024883	0.57108646	0.28834292
O3	−1.38492090	−0.59624063	0.05208896
O4	1.43837835	−0.56470384	−0.16288889
H5	0.66413987	0.58539774	1.38382683
H6	1.27759191	1.45074673	−0.03276779
H7	−1.21486713	1.48934040	0.03874836
H8	−0.62351729	0.60104693	−1.37894859
H9	−1.62595636	−0.54048047	0.98312216
H10	0.83015171	−1.31094301	−0.08527738

g$^-$G$^+$g$^-$

C1	0.23677124	0.71845818	0.59661412
C2	−0.23677124	−0.71845818	0.59661412
O3	−0.23677124	1.42044621	−0.55063638
O4	0.23677124	−1.42044621	−0.55063638
H5	−1.32770144	−0.74728429	0.64316954
H6	0.16170162	−1.23931829	1.46711198
H7	−0.16170162	1.23931829	1.46711198
H8	1.32770144	0.74728429	0.64316954
H9	0.33876887	1.18434801	−1.28487519
H10	−0.33876887	−1.18434801	−1.28487519

tTt

C1	−0.43860805	0.61464551	0.00000000
C2	0.43860805	−0.61464551	0.00000000
O3	0.43860805	1.73755717	−0.00000000
O4	−0.43860805	−1.73755717	0.00000000
H5	1.07542778	−0.60288641	0.88744548
H6	1.07542778	−0.60288641	−0.88744548
H7	−1.07542778	0.60288641	−0.88744548
H8	−1.07542778	0.60288641	0.88744548
H9	−0.09546523	2.53706794	0.00000000
H10	0.09546523	−2.53706794	0.00000000

g$^+$Tg$^-$

C1	0.00084540	0.00047103	−0.75973491
C2	−0.00084540	−0.00047103	0.75973491
O3	1.32482151	−0.00034690	−1.28249227
O4	−1.32482151	0.00034690	1.28249227
H5	0.58195628	0.84730596	1.12713764
H6	0.46494364	−0.91357045	1.13067030
H7	−0.58195628	−0.84730596	−1.12713764
H8	−0.46494364	0.91357045	−1.13067030
H9	1.71292989	−0.86417099	−1.11018124
H10	−1.71292989	0.86417099	1.11018124

tTg$^+$

C1	−0.56288057	0.49881895	−0.04388636
C2	0.56776065	−0.50850107	0.00412610
O3	−1.77604741	−0.24192692	0.04487840
O4	1.83539130	0.13223227	−0.08631595
H5	0.49812648	−1.17449291	−0.85297086
H6	0.48165893	−1.11192475	0.91055661
H7	−0.46701564	1.19918453	0.79277498
H8	−0.50232098	1.06449209	−0.97623229
H9	−2.51333513	0.36842286	−0.04828280
H10	1.99885469	0.58996815	0.74421639

g$^+$Tg$^+$

C1	0.41206602	0.63806280	−0.02700233
C2	−0.41206602	−0.63806280	−0.02700233
O3	−0.41206602	1.79697745	−0.06550343
O4	0.41206602	−1.79697745	−0.06550343
H5	−1.02937805	−0.67137536	−0.92189689
H6	−1.07853908	−0.65310314	0.84245632
H7	1.07853908	0.65310314	0.84245632
H8	1.02937805	0.67137536	−0.92189689
H9	−0.89509515	1.85066499	0.76548197
H10	0.89509515	−1.85066499	0.76548197

tG$^+$t

C1	−0.65959007	−0.36221035	0.52863732
C2	0.65959007	0.36221035	0.52863732
O3	−0.65959007	−1.28939345	−0.55115838
O4	0.65959007	1.28939345	−0.55115838
H5	1.46238479	−0.37164206	0.42146561
H6	0.77764379	0.87957610	1.48570351
H7	−0.77764379	−0.87957610	1.48570351
H8	−1.46238479	0.37164206	0.42146561
H9	−1.55608376	−1.61641367	−0.66972598
H10	1.55608376	1.61641367	−0.66972598

tG$^+$g$^+$

C1	0.68494002	0.53484283	0.30712496
C2	−0.69575343	0.53939740	−0.30519031
O3	1.40943629	−0.56874882	−0.21745027
O4	−1.48644341	−0.58149220	0.06042556
H5	−0.60467784	0.49424425	−1.38897474
H6	−1.19168896	1.47870341	−0.03897876
H7	1.17430907	1.48351373	0.06193987
H8	0.60218806	0.46704051	1.39835001
H9	2.27905417	−0.58392669	0.19348032
H10	−1.57824704	−0.58308836	1.01877310

cCt

C1	−1.02086942	−0.16099741	0.00000000
C2	−0.00000000	1.00374486	0.00000000
O3	−0.40959107	−1.43858726	−0.00000000
O4	1.31185414	0.43778116	−0.00000000
H5	−0.13798173	1.62481738	0.88597615
H6	−0.13798173	1.62481738	−0.88597615
H7	−1.65892827	−0.08154458	0.88113468
H8	−1.65892827	−0.08154458	−0.88113468
H9	0.54490025	−1.28790347	−0.00000000
H10	1.95603178	1.15132195	−0.00000000

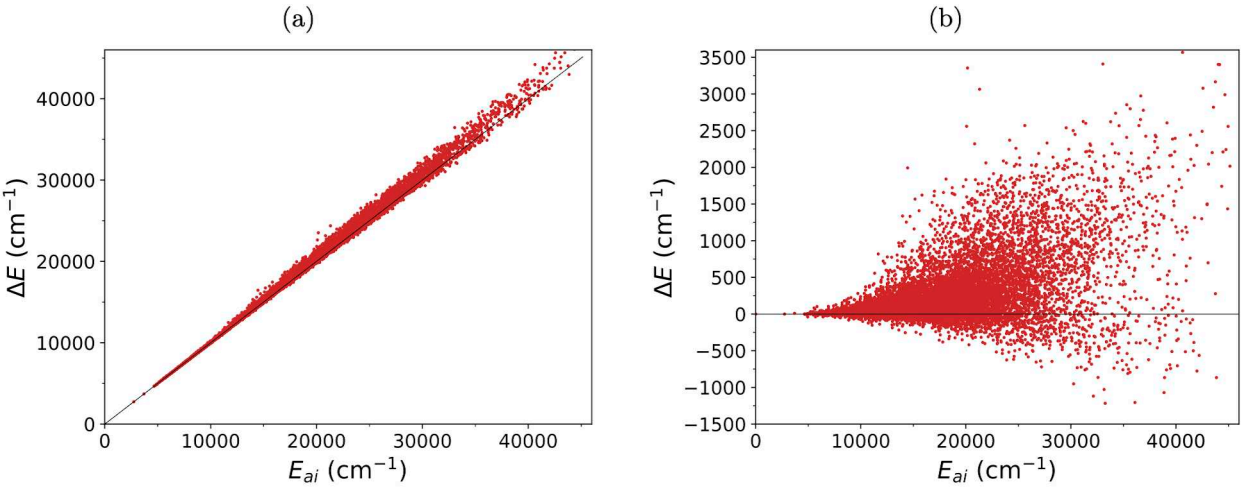

FIG. S-1. Comparison of ab initio MP2/aVTZ energies with the PES for EG truncated to quartic terms in V_b. The plots indicate large deviations at high energies, indicating the importance of including the higher order terms in the PES.

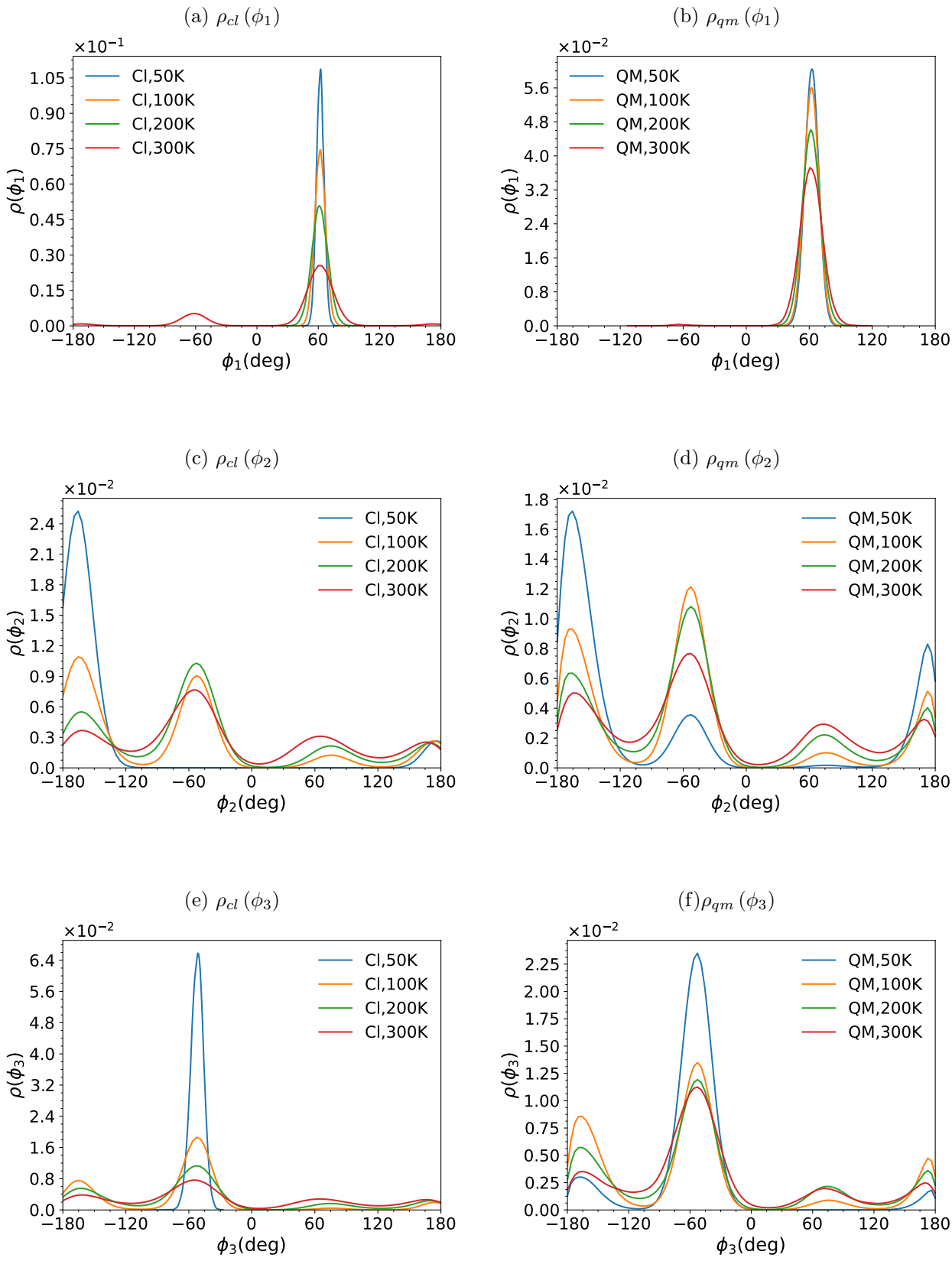

FIG. S-2. One-dimensional distributions of OCCO (ϕ_1) and the two CCOH (ϕ_2, ϕ_3) dihedrals from (a, c, e) classical and (b, d, f) PIMD simulations of EG at various temperatures.

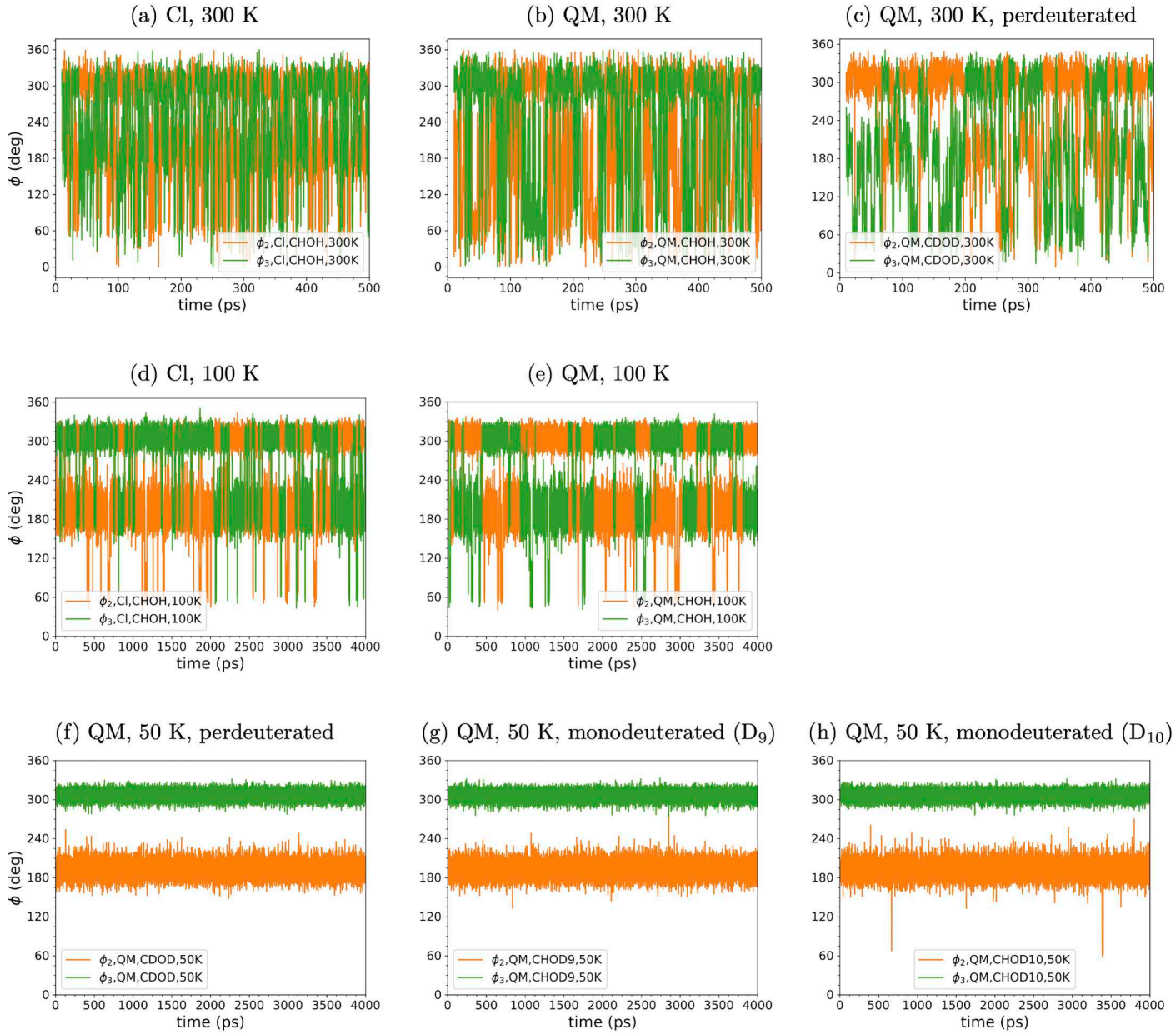

FIG. S-3. Plots of of ϕ_2 and ϕ_3 with time from classical and PIMD simulations at (a, b, c) 300 K, (d, e) 100 K, and (f, g, h) 50 K. Only where indicated above a plot, the simulations are with perdeuteration (all six H atoms replaced with D) or monodeuteration (either H_9 or H_{10} of the OH groups replaced with D). Note that the 300 K plots are shown only up to 500 ps, as the dynamics is vigorous. Plots for other temperatures are shown up to 4 ns.

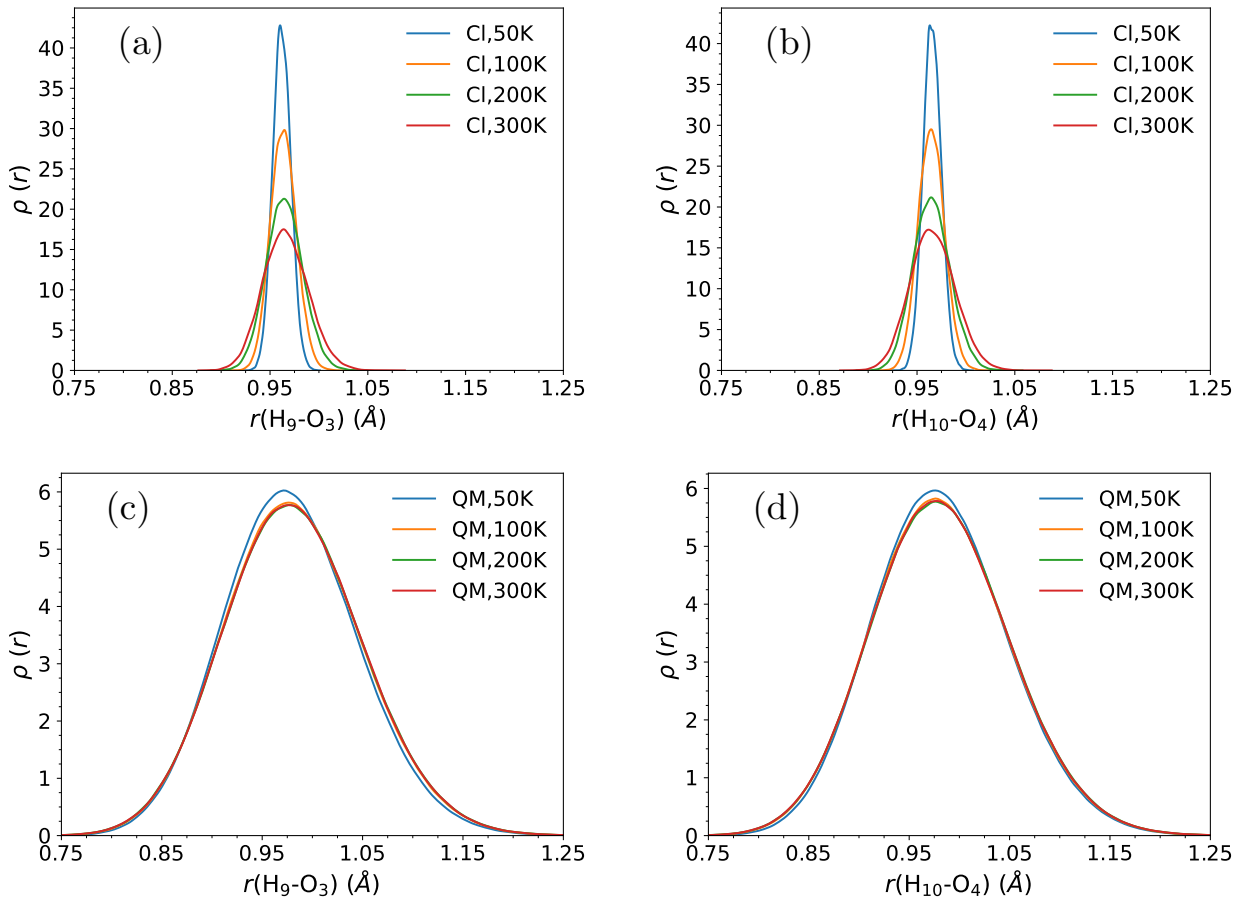

FIG. S-4. Distributions of (a, c) H_9-O_3 and (b, d) H_{10}-O_4 distances from (a, b) classical and (c, d) PIMD simulations of EG at various temperatures.

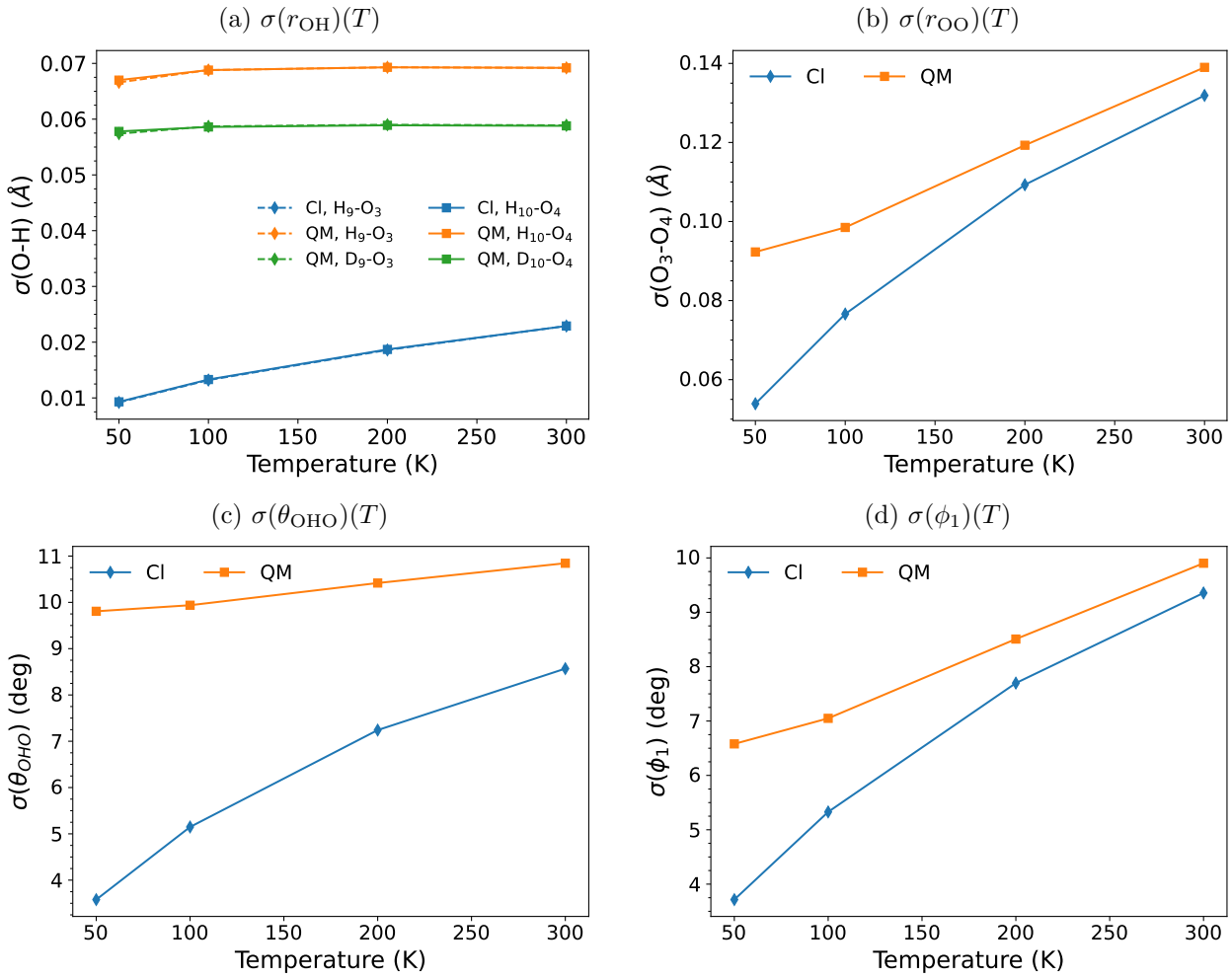

FIG. S-5. Trends of standard deviations (σ) of various internal coordinate distributions with temperature from classical and PIMD simulations. (a) Standard deviations of r_{OH} distributions from classical (blue), orange (PIMD) and green (PIMD, perdeuterated) simulation. The solid and dashed lines indicate the two different OH bonds. Standard deviations of the distributions of (b) O-O distances, (c) 'inner' O-H-O angles, and (d) OCCO (ϕ_1) dihedrals with temperature. Again, blue/orange trends are from classical/PIMD simulations.

Centroid-biased FEP $\Delta F_{qm;c}$ with H/D isotopic variation

(a) 300 K

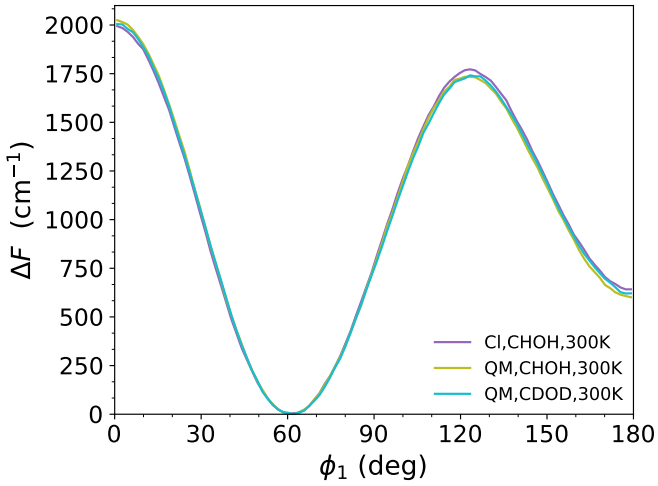

(b) 50K

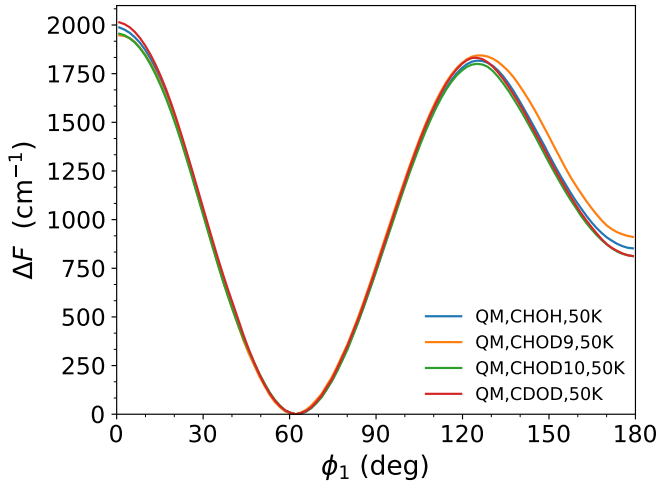

(c) **Bead-biased FEP** $\Delta F_{qm;b}$
with H/D isotopic variation at 300 K and 50 K

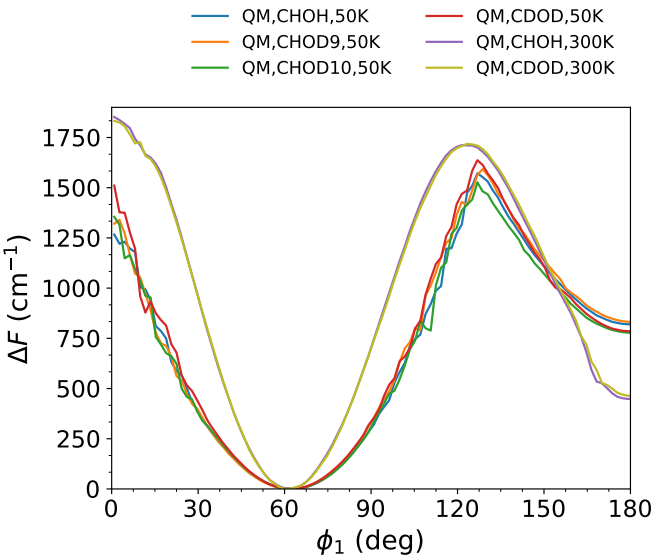

FIG. S-6. Additional free energy profiles for EG. (a) Centroid-biased free energy profiles, $\Delta F_{qm;c}(\phi_1) = F_{qm,c}(\phi_1) - F^{min}_{qm,c}$, at 300 K obtained by path integral umbrella sampling simulations along ϕ_1, both without and with deuteration. Classical simulation results are shown alongside. (b) Same as (a) but at 50 K. (c) Variation of $\Delta F_{qm;b}(\phi_1)$ without and with H/D isotopic substitution at both 50 K and 300 K. *Legend notation:* CHOH ≡ no isotopic substitution. CHOD9 and CHOD10 ≡ monodeuration (D_9 and D_{10}, respectively); see Fig. 1 for atom numbering. CDOD ≡ perdeuteration.

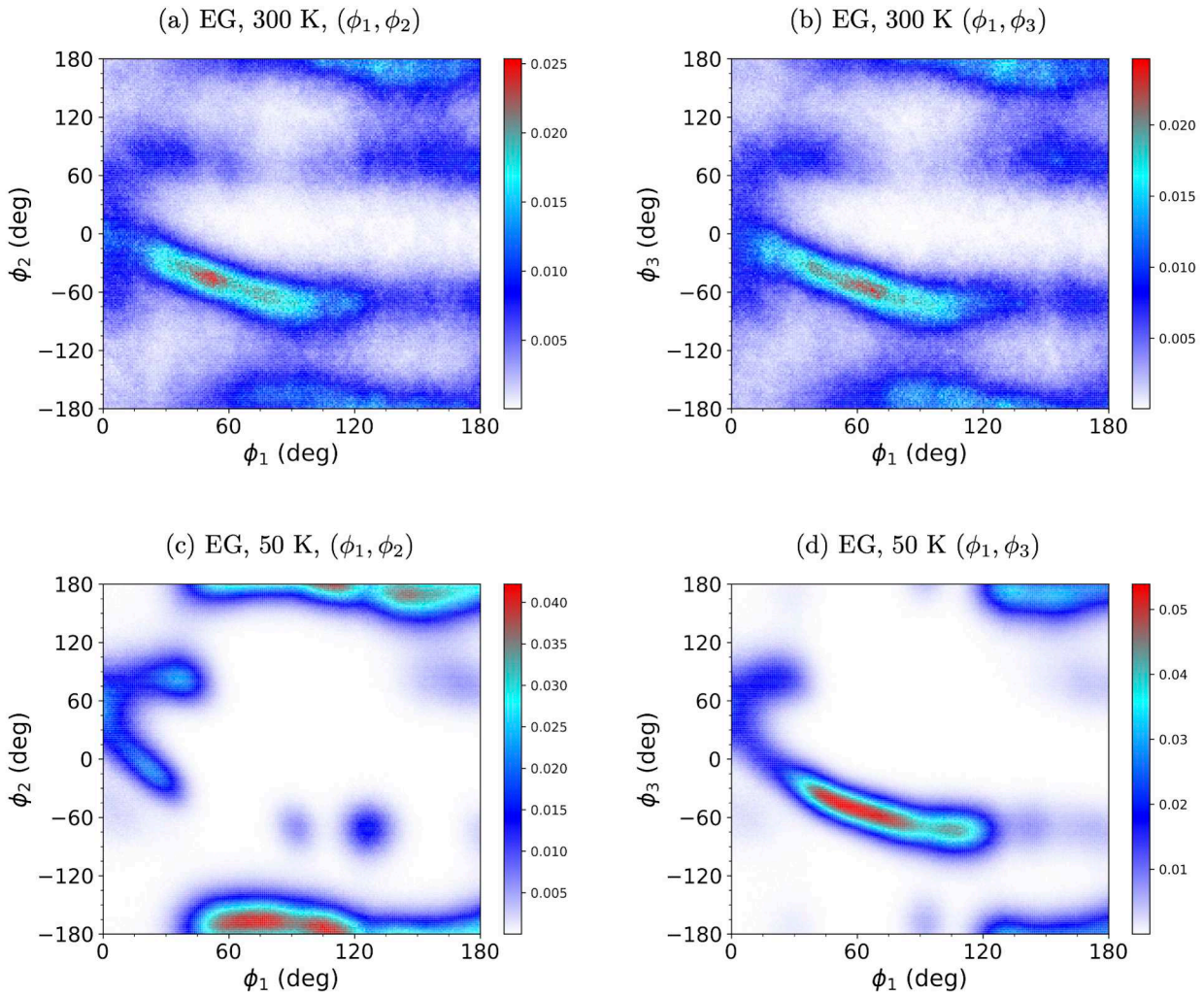

FIG. S-7. Distribution of centroid (ϕ_1, ϕ_2, ϕ_3) values obtained via umbrella sampling simulations along the OCCO dihedral ϕ_1 at both 50 K and 300 K for undeuterated EG.

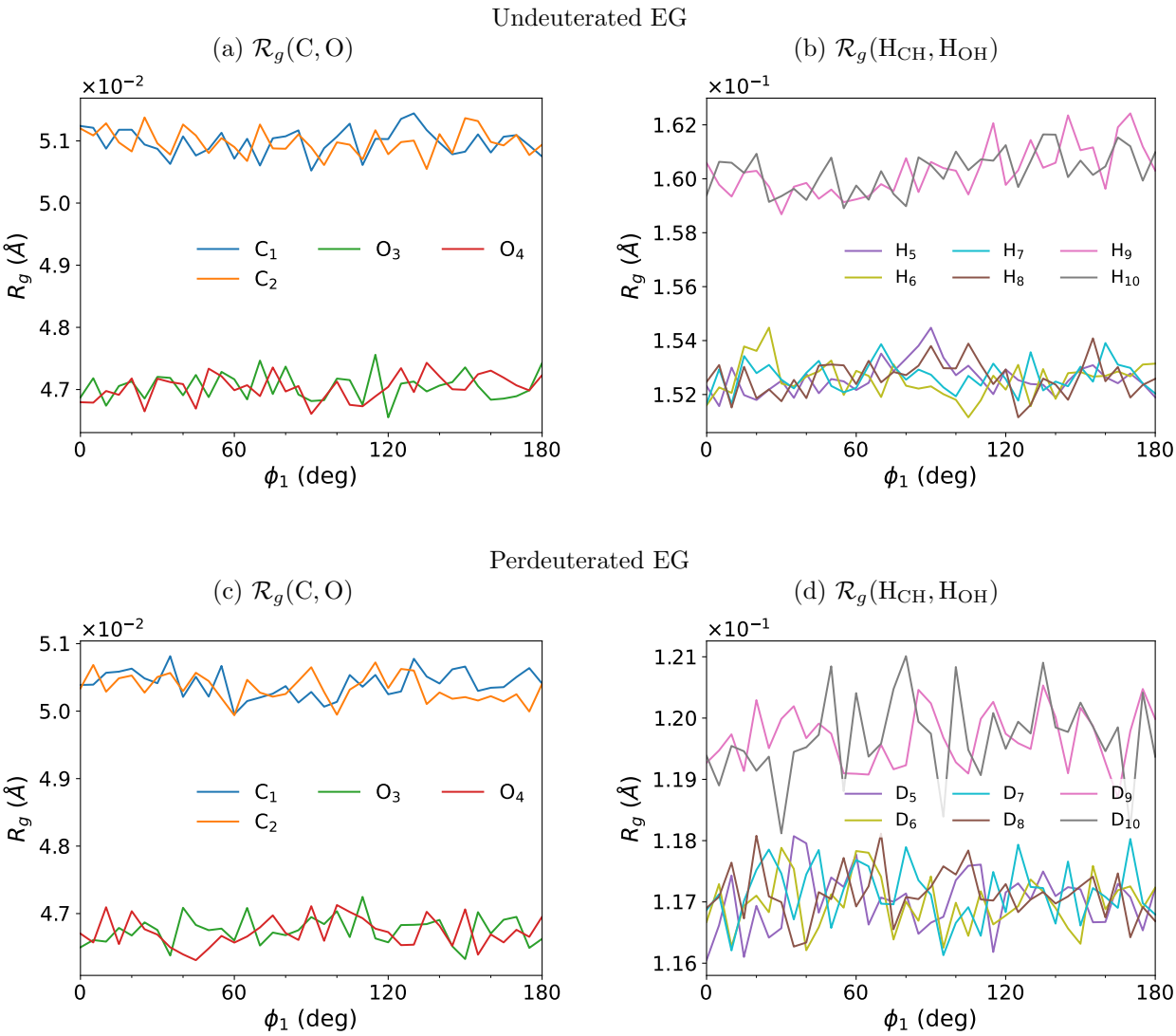

FIG. S-8. Mean radii of gyration $\mathcal{R}_g$ of atoms in undeuterated and deuterated EG at 300 K as a function of ϕ_1. See Fig. 1 for the atom numbers.

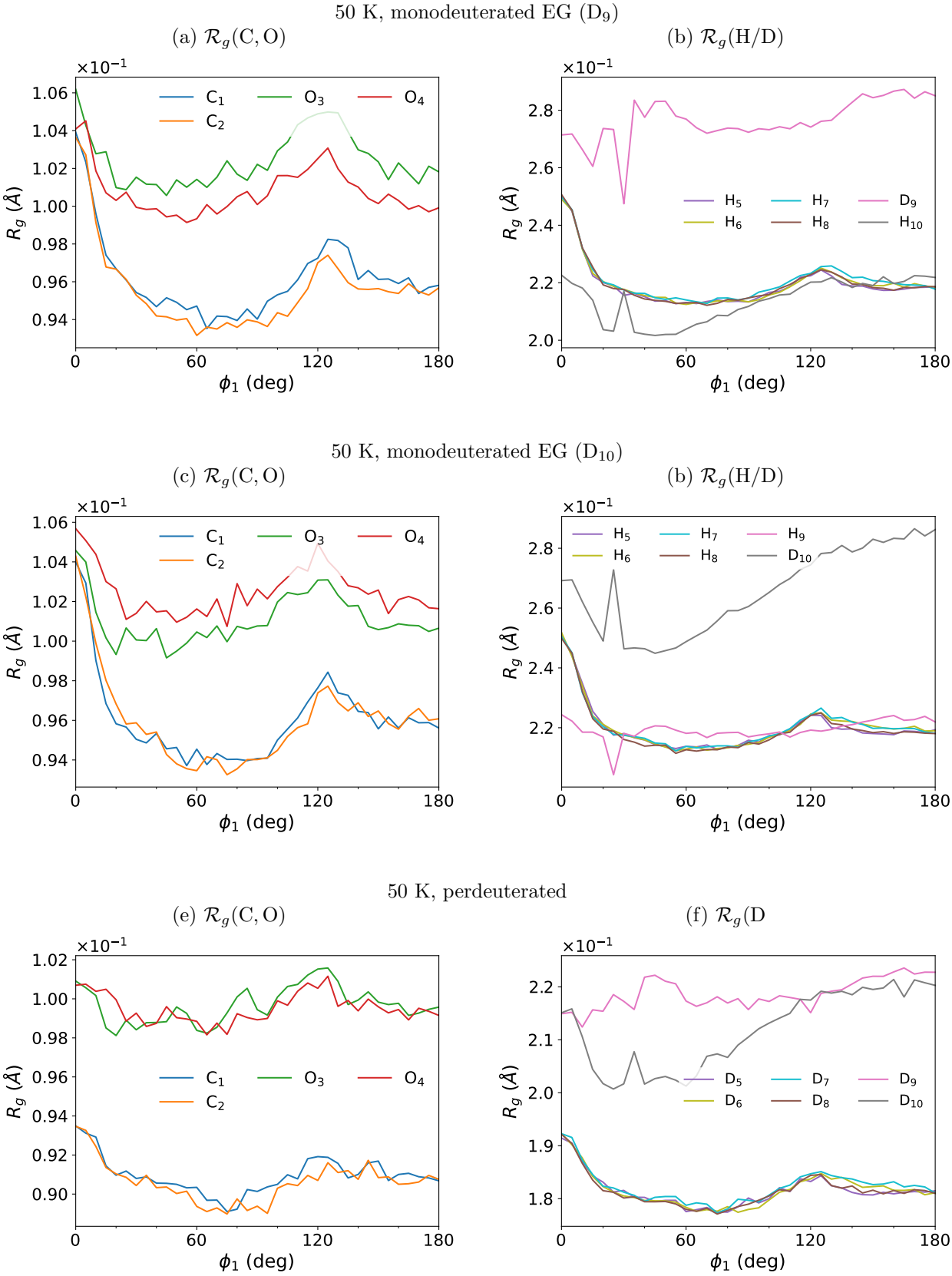

FIG. S-9. Mean radii of gyration $\mathcal{R}_g$ of atoms in deuterated EG at 50 K as a function of ϕ_1. See Fig. 1 for the atom numbers.

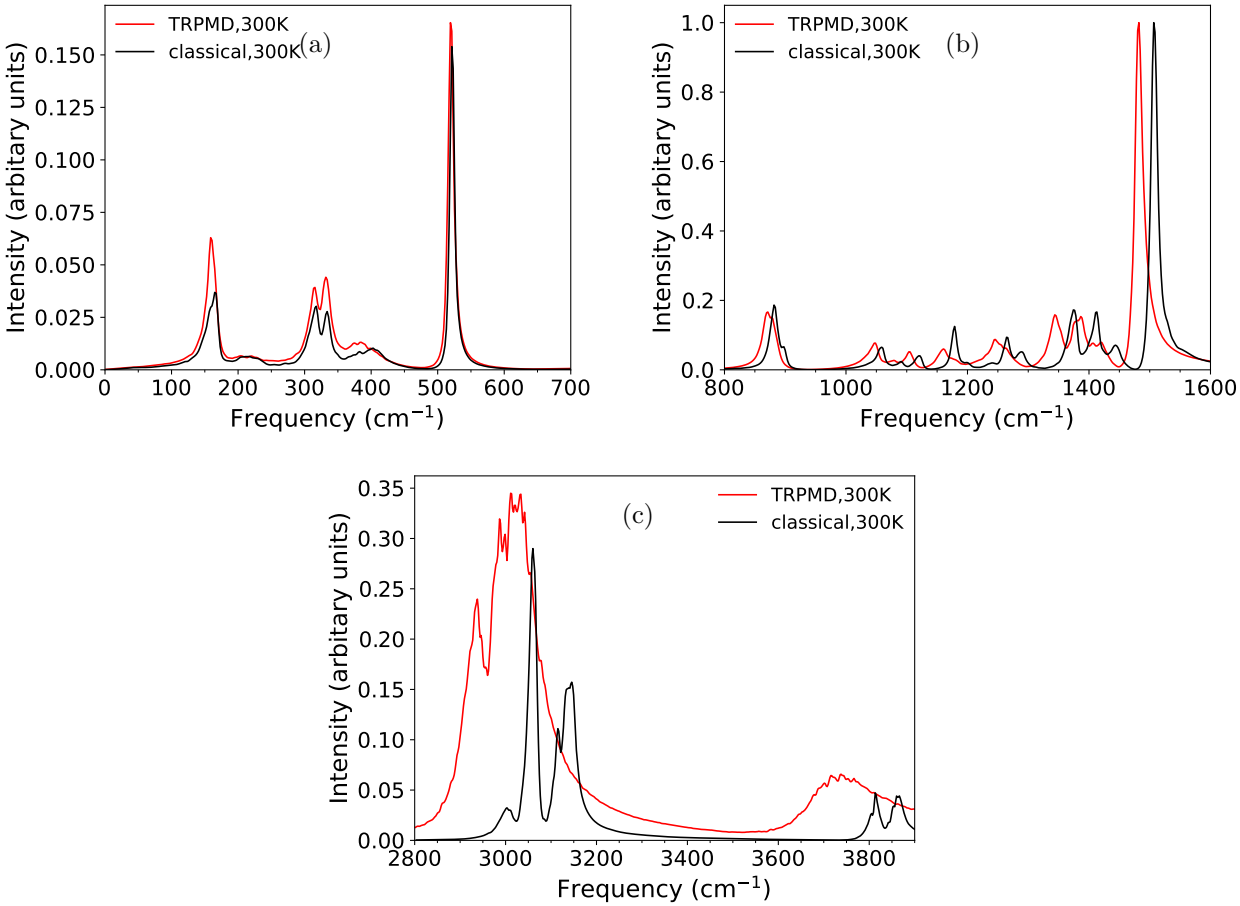

FIG. S-10. Comparison of classical and T-RPMD power spectra at 300 K.